ELSEVIER

Journal of Crystal Growth 235 (2002) 25–34

JOURNAL OF CRYSTAL GROWTH

www.elsevier.com/locate/jcrysgro

MOVPE process development for 650 nm VCSELS using optical in-situ techniques

M. Zorn[a,*], K. Haberland[b,c], A. Knigge[a,1], A. Bhattacharya[a,2], M. Weyers[a], J.-T. Zettler[b,c], W. Richter[b]

[a] Ferdinand-Braun-Institut für Höchstfrequenztechnik, Albert-Einstein-Str. 11, D-12489 Berlin, Germany
[b] Technische Universität Berlin, Institut für Festkörperphysik, Sekr. PN 6-1, Hardenbergstr. 36, D-10623 Berlin, Germany
[c] LayTec GmbH, PN 5-7, Hardenbergstr. 36, D-10623 Berlin, Germany

Received 28 June 2001; accepted 27 September 2001
Communicated by J.B. Mullin

Abstract

In this paper we report on the optimization and control of key layer properties of visible vertical cavity surface emitting laser (VCSEL) for emission at wavelengths around 650 nm by means of an optical real-time sensor allowing for both spectroscopic reflectance and reflectance anisotropy measurements. In contrast to conventional ex-situ characterization the in-situ sensor yields information on properties like thickness, composition and doping for all buried layers, especially the lower distributed Bragg reflector which has a strong influence on the final device performance. Using in-situ sensor-based optimization of the growth process 650 nm VCSEL devices with a record-high continuous-wave output power of 3 mw at room temperature have been fabricated. © 2002 Elsevier Science B.V. All rights reserved.

PACS: 81.05.Ea; 81.15.Gh; 42.55.Px; 78.40.Fy; 78.66.Fd

Keywords: A3. Laser epitaxy; A3. Metalorganic vapor phase epitaxy; B2. Semiconducting III–V materials; B3. In-situ reflectance; B3. Laser diodes; B3. Reflectance anisotropy spectroscopy

1. Introduction

Vertical cavity surface emitting lasers (VCSELs) offer significant advantages over conventional edge emitting lasers, such as circular beam profiles, dynamic single-frequency operation, ease of two-dimensional array fabrication and the possibility of wafer-scale testing [1,2]. High-performance visible-wavelength VCSELs emitting at a wavelength of 650 nm would impact emerging technologies such as high-density optical storage systems, high-definition laser printing and especially optical communication systems based on plastic optical fibers, for which absorption losses have a minimum at a wavelength of 650 nm. Visible wavelength VCSELs typically consist of n- and p-type doped AlGaAs distributed Bragg reflectors

*Corresponding author. Tel.: +49-30-6392-2676; fax: +49-30-6392-2685.
E-mail address: zorn@fbh-berlin.de (M. Zorn).
[1] nee: A. Oster.
[2] Present address: Solid State Electronics Group, Tata Institute of Fundamental Research, Homi Bhabha Road, Mumbai 400 005, India.

0022-0248/02/$ - see front matter © 2002 Elsevier Science B.V. All rights reserved.
PII: S 0 0 2 2 - 0 2 4 8 (0 1) 0 1 7 5 8 - 4

(DBRs) sandwiching a "one-λ" thick AlInGaP cavity containing strained InGaP quantum wells (QWs). With about 200 semiconductor layers in the total stack the VCSEL structure is in consequence very thick ($\approx$8–9 μm). Due to their complexity these VCSELs raise particularly difficult issues in the crystal growth by metal-organic vapour phase epitaxy (MOVPE) [3]. Maintaining tight control over the layer thickness over a relatively long process time is therefore vital. The key criterion here is that the peak reflectance wavelength of both DBR mirrors and the resonance wavelength of the cavity all must be adjusted precisely to the same desired value. In addition, tight control is also needed for the doping level, the layer composition and the interface grading of the DBRs. Therefore, in this work we focus on the optimization and control of MOVPE growth for 650 nm emitting VCSELs by means of an optical in-situ sensor that allows combined reflectance and reflectance anisotropy spectroscopy (RAS) [4,5] measurements in a commercial MOVPE reactor.

Optical techniques have been used for in-situ investigations of DBR growth since the early stages of VCSEL development. In 1993 the molecular beam epitaxy based growth of DBR mirrors was studied in-situ by spectroscopic ellipsometry (SE) [6]. Ellipsometry, however, is not implementable in production line processes using multi-wafer growth reactors and substrate rotation. This is primarily because SE requires that the angle of incidence is precisely adjusted (with an accuracy better than 0.01°). Therefore, single wavelength pyrometry [7,8] and reflectance measurements [9] in conjunction with a virtual interface model [10] have seen greater application to measure the growth rate in-situ. RAS has been used for investigating the growth of InGaP [11], the n- and p-type doping of AlInP [12] as well as the process of intrinsic carbon (C) doping in GaAs [13].

In this paper we report on a comprehensive in-situ study of VCSEL growth in MOVPE that uses two normal incidence, fully spectroscopic optical in-situ techniques: reflectance and RAS. The normalized reflectance gives information on the reflectance wavelength and composition of the DBRs, the resonance wavelength of the cavity and the cap layer thickness. The RAS mode of the sensor assesses the doping level of the respective layers and both the surface stoichiometry and surface morphology during growth. The data obtained in-situ are compared and correlated to both the ex-situ measured data of the layer structures as well as the electro-optic properties of the final VCSEL device.

2. Experimental procedure

All epitaxial layer structures discussed in this work were grown in Aixtron 200 and Aixtron 200/4 low-pressure MOVPE systems featuring gas foil rotation of the wafers. The sources used include trimethylgallium (TMGa), trimethylaluminium (TMAl), trimethylindium (TMIn), arsine (AsH_3) and phosphine (PH_3). Triethylgallium was used for AlGaAs layers containing very small amounts of Ga ($<5\%$). Silicon (Si) from Si_2H_6 was used as n-type dopant. Intrinsically incorporated C and zinc (Zn) from dimethylzinc were utilized for p-type doping. Intrinsic C doping is based on the incorporation of C from only partially decomposed TMGa or TMAl by growth at low V/III ratios [13]. It was found that the series resistance of the VCSEL structure can be lowered when the commonly used Zn is replaced by C as p-type dopant [14]. The growth pressure was 100 or 150 mbar and a typical growth temperature was 770°C. Epiready n^+ GaAs (1 0 0) substrates misoriented 6° towards [1 1 1]A were used.

The MOVPE systems were equipped with low-strain UV transparent viewports for normal incidence optical access and with a corresponding hole in the liner-tube. The in-situ measurements were performed with a LayTec EpiRAS-200[3] spectrometer that allows combined RAS and reflectance (R) measurements under standard device growth conditions [15,16]. RAS measurements are highly sensitive to the optical anisotropy induced by the surface reconstruction and were used to ensure perfect surface quality during

[3] Technical description of EpiRAS-200, LayTec GmbH, http://www.laytec.de.

growth. RAS measures the difference in reflectance for linear polarized light along the two principal axis on the surface. For a (0 0 1) surface the RAS signal is given by

$$\frac{\Delta r}{r} = 2\frac{r_{[\bar{1}\,1\,0]} - r_{[1\,1\,0]}}{r_{[\bar{1}\,1\,0]} + r_{[1\,1\,0]}}, \quad (1)$$

where $r_{[1\,1\,0]}$ and $r_{[\bar{1}\,1\,0]}$ are the complex reflectances of light polarized linearly along the indicated directions within the surface [5]. For the in-situ growth studies reported here it is sufficient to discuss only the real part of the spectra $|\mathrm{Re}(\Delta r/r)|$ [17].

The reflectance $R = r \cdot r^* = |r|^2 = I_r/I_i$ is by definition the ratio between the reflected light intensity I_r and the incident intensity I_i. When R is measured ex-situ, beam-splitting techniques are usually applied for detecting both I_i and I_r synchronously. For in-situ measurements, influenced, e.g. by varying window absorbance, this is not feasible. Therefore, we introduced the normalized reflectance R/R_{ref}, which is the actual reflectance of the growing layer stack divided by the reflectance of a well-known reference sample inside the reactor. In this work the GaAs substrate reflectance $R_{ref} = R_{GaAs}$ was measured prior to the growth of the VCSEL structure and used thereafter as reference. As a consequence the measured parameter R/R_{ref} could be determined with an accuracy better than 0.2%. This normalized reflectance is independent from the spectrum of the light source, the detector sensitivity, the transmission of the window, etc. Thus, the normalized reflectance can be simulated by a multilayer growth model based on a high-temperature dielectric function database. In addition, similarly and complementarily to RAS, the normalized reflectance R/R_{ref} can be directly used for the comparison of growth processes in different growth systems.

With the EpiRAS type of sensor used in this work, measurements can be either performed spectroscopically between 248 nm (5.0 eV) and 826 nm (1.5 eV) or time resolved at a fixed wavelength. The maximum time resolution depends on the wafer rotation frequency, since one full wafer rotation has to be measured for each data point. For the growth parameters used in this work, the time resolution for the combined R/RAS single wavelength measurement was about 2 s. When only the reflectance was analyzed the time resolution was better than 1 s.

After growth of the VCSEL structures ex-situ characterization has been performed by electroluminescence, X-ray diffraction and spectroscopic reflectance measurements.

Both the time-resolved in-situ reflectance measurements and the post-growth ex-situ reflectance spectra have been simulated using the commercially available thin-film analysis software AnalysR.[4] Dielectric function data have been taken either from a previously published database [18] or have been determined by our own reference experiments [19].

Finally, the layer structures were processed into air-post/oxide confined mesa-type VCSELs of 30–60 μm diameter which were characterized for their device properties under pulsed and continuous-wave (cw) excitation [20].

3. Results and discussion

3.1. VCSEL structure

Fig. 1 shows a sketch of the VCSEL structure studied in this work. It consists of a n-doped bottom DBR with 55.5 pairs of $Al_{0.50}Ga_{0.50}As$/AlAs and a cavity with three InGaP QWs embedded in AlInGaP. The p-doped top DBR consists of 35 pairs of $Al_{0.50}Ga_{0.50}As/Al_{0.95}Ga_{0.05}As$ except for the third pair, which is $Al_{0.50}Ga_{0.50}As/Al_{0.98}Ga_{0.02}As$ to facilitate the formation of an aperture by wet oxidation. Graded interfaces have been introduced in the top p:DBR to reduce its series resistance [14,21]. In the following sections the growth of different regions of the VCSEL structure will be discussed in detail, focussing on the information obtained from the optical RAS/reflectance data.

[4] AnalysR, simulation and analysis software, LayTec GmbH, http://www.laytec.de.

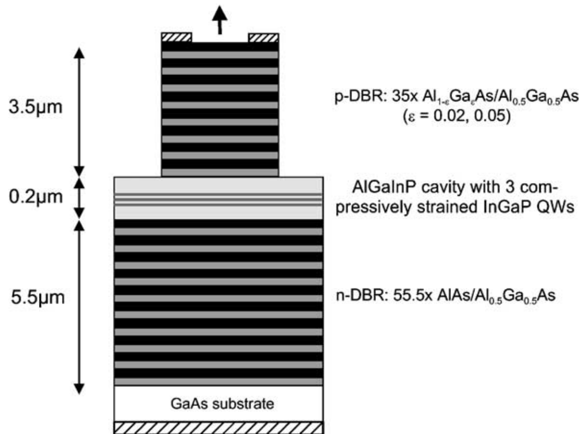

Fig. 1. Sketch of the VCSEL structure emitting at a wavelength around 650 nm.

3.2. Doping level of the DBRs

Fig. 2a shows representative reflectance anisotropy (RA) spectra for the n-doping of $Al_{0.55}Ga_{0.45}As$ with silicon. With increasing doping concentration the whole spectrum shifts to lower RA values with the strongest response being obtained in the region of high photon energies. Fig. 2b shows RA spectra for intrinsically C p-doped $Al_{0.40}Ga_{0.60}As$ layers. These spectra, taken under AsH_3 stabilization at 770°C, display an increase of the RA values with increasing doping concentration. When choosing an optimum wavelength for monitoring the doping process in-situ one has to consider trade-offs between surface sensitivity and sensitivity to changes in doping level. The penetration depth of light decreases with decreasing wavelength which implies that the sensitivity of the RA signal to the growing uppermost layer increases at shorter wavelength (higher photon energy). Therefore, 310 nm (4.0 eV) was chosen as a suitable wavelength for monitoring the doping concentration during the VCSEL growth even though for p-type doping a higher sensitivity could be reached at 500 nm (2.5 eV). Due to the low penetration depth ($\approx$10 nm) at 310 nm and because this wavelength is sufficiently separated from the reflectance stop band of the 650 nm VCSEL ($\approx$700 nm at growth

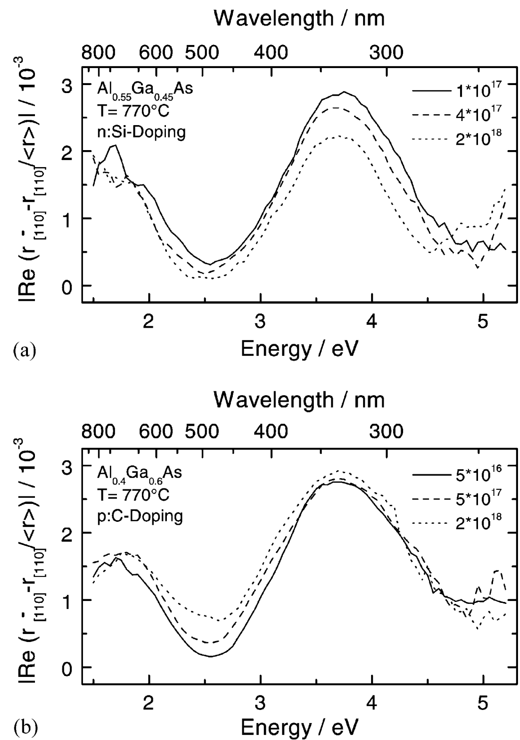

Fig. 2. Dependence of RA signal on doping concentration for (a) n-type doping of $Al_{0.55}Ga_{0.45}As$ using silicon and (b) p-type doping of $Al_{0.40}Ga_{0.60}As$ using carbon.

temperature), the influence of Fabry-Perot (FP) oscillations on the RA signal is relatively small.

Fig. 3a shows the time-resolved RA monitoring of the complete VCSEL growth process at 310 nm (4.0 eV). The respective doping types and doping levels can be seen in the corresponding levels of the RA signal for both the p- and n-type DBRs. The RA response to the doping level is different for the AlAs and AlGaAs layers and there is also a residual influence of FP interferences at the onset of the growth of a new layer. The mean level of the RA signal (dashed lines in Fig. 3b) corresponds to the characteristic doping level in both types of DBRs. In Fig. 3a it can also be resolved that in this particular VCSEL structure the fifth layer of the top p:DBR (dashed circle in Fig. 3a) has a higher RA signal caused by an intentionally higher doping level.

Fig. 3b shows a magnified section of the RA transient for the first 20 layers of a top p:DBR.

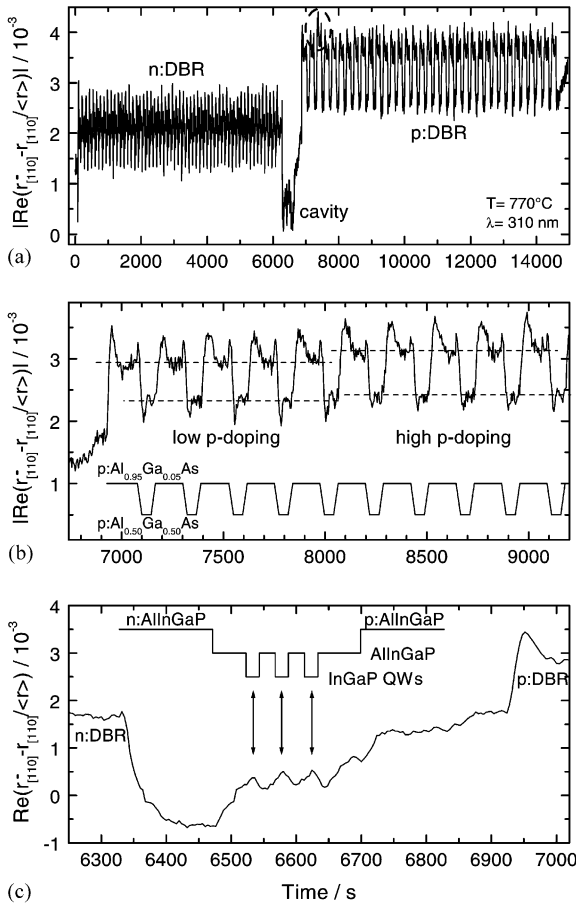

Fig. 3. (a) RA transient taken at 310 nm (4.0 eV) during growth of a complete VCSEL device. The fifth p:DBR layer having a higher doping level is indicated by the dashed circle. (b) Section of a RA transient showing the growth of a p:DBR of a VCSEL structure with lower doping of the first five mirror pairs. (c) Magnification of a transient showing the growth of the AlInGaP cavity including the three InGaP QWs (switching sequences as indicated). In (c) the sign of the RAS signal has been corrected for clarification.

The related switching sequence is indicated in the lower part of the figure. In this special case the doping concentration was increased after the growth of the first five mirror pairs (first 10 layers) by approximately a factor of two. This change in doping concentration can clearly be resolved in the RA signal for both $Al_{0.95}Ga_{0.95}As$ and $Al_{0.50}$-$Ga_{0.50}As$ even though in the latter case the influence on the RA response is slightly smaller.

3.3. DBR interface grading

Due to low hole mobilities and high valence band offsets the interfaces in the p:DBR are particularly crucial for the series resistance and therefore for the performance of the VCSEL device. A method to reduce this series resistance is the introduction of compositional grading of the DBR interfaces [14,21]. Fig. 4a and b shows time-resolved normalized reflectance measurements at 310 nm (4.0 eV) during growth of a VCSEL structure. In contrast to the RA measurements discussed above the reflectance signal at this photon energy is not sensitive to doping effects. Here the measured reflectance signals are dominated by the composition. Fig. 4a shows the growth of five pairs of layers of the bottom DBR having abrupt interfaces. The signals exhibit FP-oscillations that attenuate quickly since the material is strongly absorbing at this photon energy. The transient in Fig. 4a shows perfect periodic behavior after the first pair, which has a different starting level, because it was grown on GaAs. The switching from AlAs to AlGaAs and vice versa can clearly be identified by a strong and sharp peak and valley signature in the respective FP-oscillations, caused by the superposition of light reflected at the growth surface and at the first buried interface. These FP-oscillations, however, quickly dampen out due to the high absorption of the material at this wavelength.

Fig. 4b shows five pairs of layers of a top DBR featuring a 10 nm graded layer at the interfaces. For these graded interfaces it can be clearly seen that the respective FP-oscillations are much smaller. These effects can be seen in more detail in Fig. 4c where the reflectance response of a single layer pair is given for both the abrupt and the graded case. Fig. 4d shows a simulation of the reflectance transient based on a multi-layer model where the graded interface is simulated by five transition layers (each 2 nm thick) with changing composition. The simulation shows where differences in the reflectance response of DBRs having abrupt and graded interfaces are to be expected. Especially when switching from AlAs to AlGaAs, the amplitude of the first maximum of the FP-oscillation is highly sensitive to the abruptness of

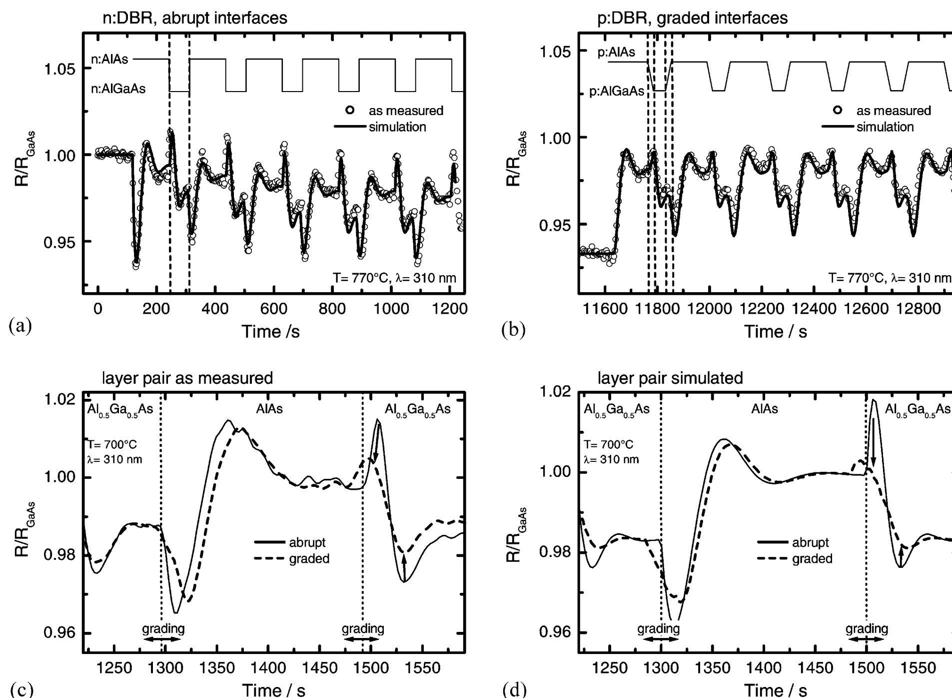

Fig. 4. (a) Normalized reflectance transients taken during growth of DBRs having (a) abrupt interfaces (n:DBR) and (b) graded interfaces (p:DBR). In (c) the details of a measured two-layer sequence are directly compared for both cases. (d) Respective simulation for a two-layer sequence having abrupt and graded interfaces.

the interface and nearly vanishes in the graded case. Grading causes a general reduction of the related maximum–minimum signature and results in a significantly broadened FP-oscillation. For the AlGaAs/AlAs interface basically the same grading induced changes can be seen even though the effects are smaller in this case. All these grading induced effects simulated in Fig. 4d are present in the measured transients in Fig. 4c as well. However, they are not as pronounced as expected. We believe that this is related to a non-ideal realization of the grading perhaps due to non-ideal control characteristics of the mass flow controllers.

3.4. AlInGaP/InGaP cavity

The cavity is formed by n-, p- and undoped AlInGaP layers containing the very thin InGaP QWs. Fig. 3c shows the enlarged part of a RA transient taken during the growth of the cavity. The corresponding switching sequence is indicated in the upper part of the figure. At first it can clearly be seen that the very thin InGaP QWs layers can also be resolved. This is caused by the fact, that InGaP [11] has a different optical response than undoped AlInGaP [12] at this particular wavelength. In addition, it is expected that interface-related signatures also contribute to the measured RA response of the QWs. Secondly, the different doping levels during the growth of the AlInGaP can be distinguished. The doping level in the AlGaInP cavity is critical in determining the leakage current in visible VCSELs and thus the device performance. The cavity growth starts with the growth of n-doped AlInGaP which shows only a small RA signal. The RA signal then increases when undoped AlInGaP is grown in the vicinity of the QWs. Finally, when starting the growth of the p-doped AlInGaP the RA signal increases again.

The doping related RA response observed for AlGaInP is very similar to that of AlInP reported previously [12].

3.5. Growth of the GaAs top contact layer

For optimum performance of a VCSEL it is very important that every layer in the stack is grown to its desired thickness. This also holds for the p^{++}-doped GaAs top contact layer where due to the low As flux stable growth conditions are difficult to achieve. Since this layer is doped to $4\times10^{19}\,cm^{-3}$ by intrinsic C doping, the contact layer has to be grown at a very low V/III ratio (≈ 1) and at a low temperature ($\approx 550°C$). Fig. 5 shows the respective reflectance transient of the p^{++}-doped GaAs top contact layer growth. When the growth is initiated at 15,580 s, a characteristic decline in reflectance can be observed at the stop-band wavelength. After passing to a minimum reflectance close to zero at a GaAs layer thickness of about 40 nm, the reflectance recovers until a reflectance of $\sim 78\%$ is reached again. This reduced reflectance level is caused by the absorption in the p^{++}-doped GaAs layer. The growth was stopped immediately after the reflectance signal saturated (15740 s).

3.6. Device properties and DBR alignment

Fig. 6 shows the almost indistinguishable post-growth room-temperature reflectance spectra of two VCSEL structures A and B. Both spectra exhibit a very similar line shape varying only in a small difference in the center wavelength of the stop-band edges. For both samples the cavity resonance can be clearly resolved exactly at 650 nm. However, after device processing the properties of the two VCSEL structures are remarkably different. Table 1 shows that sample B has better key properties like threshold-current density and output power as compared to sample A. This is also supported by Fig. 7 where the cw-power-current and the voltage-current characteristics of the two devices with 37 μm mesa diameter and an oxide aperture of 8 μm emitting at 650 nm are compared. The voltage-current characteristics are similar for both structures. This shows that the electrical properties of both devices are the same as expected from the growth process. However, when

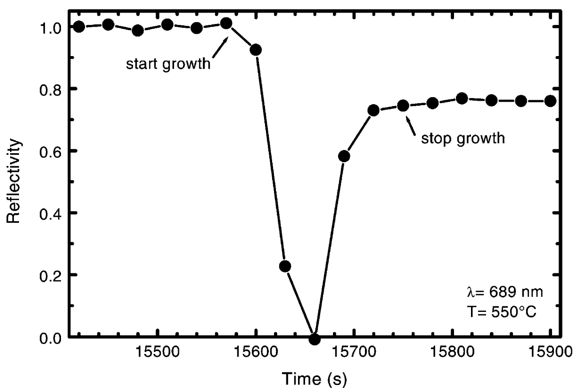

Fig. 5. Reflectance transient taken during growth of the p^{++}-GaAs cap layer.

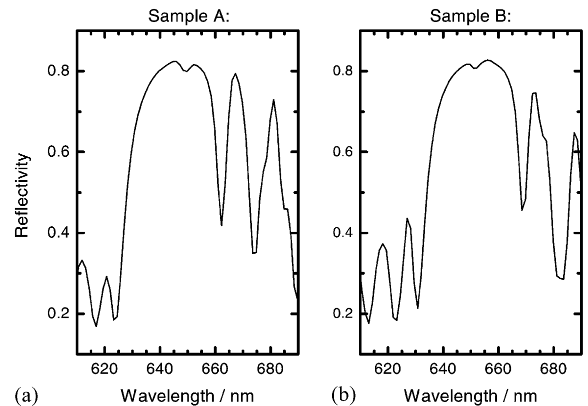

Fig. 6. Comparison of the ex-situ reflectance spectra of the two different VCSEL samples A and B having nominally the same structure but different electro-optic properties (see Table 1).

Table 1
Electro-optic properties of the VCSELs studied for lasing at 647 nm

	Threshold-current density (kA/cm^2)	Pulsed output power (mW)	CW output power
VCSEL A	10	0.34	No cw operation
VCSEL B	6	0.8	0.16 mW (at 650 nm)

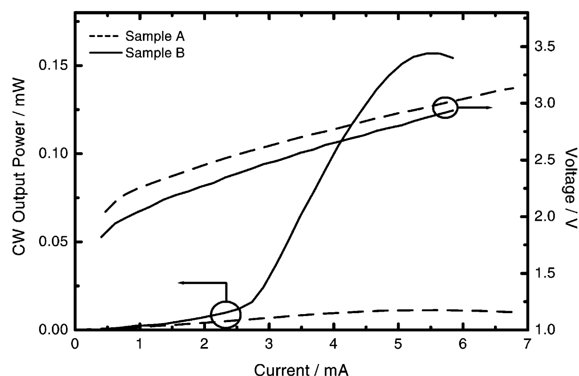

Fig. 7. CW-power-current and voltage-current characteristics of the two VCSEL samples taken at 10°C.

comparing the cw-power-current characteristics of both structures it can be seen that sample A shows only spontaneous emission while sample B clearly shows laser operation in cw mode. This is a strong indication that the optical properties of the structures are different which, however, cannot be inferred from the ex-situ reflectance measurements discussed above (Fig. 6). A detailed analysis of the full spectroscopic normalized reflectance R/R_{GaAs} fingerprint of the VCSEL growth (Figs. 8 and 9, color coded as indicated) taken in-situ clearly reveals the reason for the different performance of the two structures. In Fig. 8 the development of the reflectance of the lower and upper DBR of VCSEL-A and VCSEL-B can be directly compared. In Fig. 9 the complete reflectance fingerprint as measured throughout a full VCSEL growth process (Fig. 9a) is compared to a model calculation (Fig. 9b). During growth of the lower DBR a strong reflectance region—the so-called stop band—shows up at around 700 nm at growth temperature. The dashed lines indicate the edges of this stop band. After the growth of the cavity and of the first layers of the upper DBR a characteristic minimum clearly can be seen at 685 nm. This is the so-called cavity resonance (dash-dotted line). The cavity resonance feature gradually disappears during the continuing growth of the upper DBR because it shrinks in magnitude and cannot be resolved anymore at growth temperature due to thermal broadening. Finally, as the device cools down after growth the maximum of the reflectance shifts to the desired value of around 650 nm at room temperature.

For VCSEL A (Fig. 8a) there is an obvious mismatch in the center wavelength between the lower DBR and the upper DBR (indicated by the dashed lines at the edges of the respective DBR). Fig. 8b shows the corresponding fingerprint taken during growth of VCSEL B. The general appearance of the reflectance response is similar. In contrast to VCSEL A, however, for VCSEL B the center wavelengths of the lower and upper DBR stop bands match perfectly. Therefore it can be concluded that the alignment tuning of the lower and upper DBR can be correlated to the different electro-optic performance of both VCSELs.

Furthermore, after a systematic application of such in-situ studies to the growth of different VCSEL structures it was possible to produce high-performance 650 nm VCSELs. In pulsed operation the threshold current density is as low as 1.7 kA/cm^2. For VCSELs with oxide aperture a maximum output power in cw operation of about 3 mW at room temperature has been achieved [22]. This is, to the best of our knowledge, better than the previously published values [23,24].

4. Summary

For monitoring and optimizing the growth of VCSEL structures emitting at 650 nm an optical in-situ sensor featuring a combined spectroscopic measurement of the normalized reflectance and the RA was used. It was demonstrated that the reflectance of the lower and the upper DBRs, the cavity resonance wavelength, the doping level and the interface grading of the DBRs and the contact layer thickness can all be measured and controlled in-situ.

A comparison between in-situ measurement and simulation of the DBR reflectance response enabled a detailed understanding of the very different optical response of graded and abrupt interfaces.

Furthermore, it has been shown that a small detuning of the DBR stop bands, which is not detectable by any nondestructive ex-situ character-

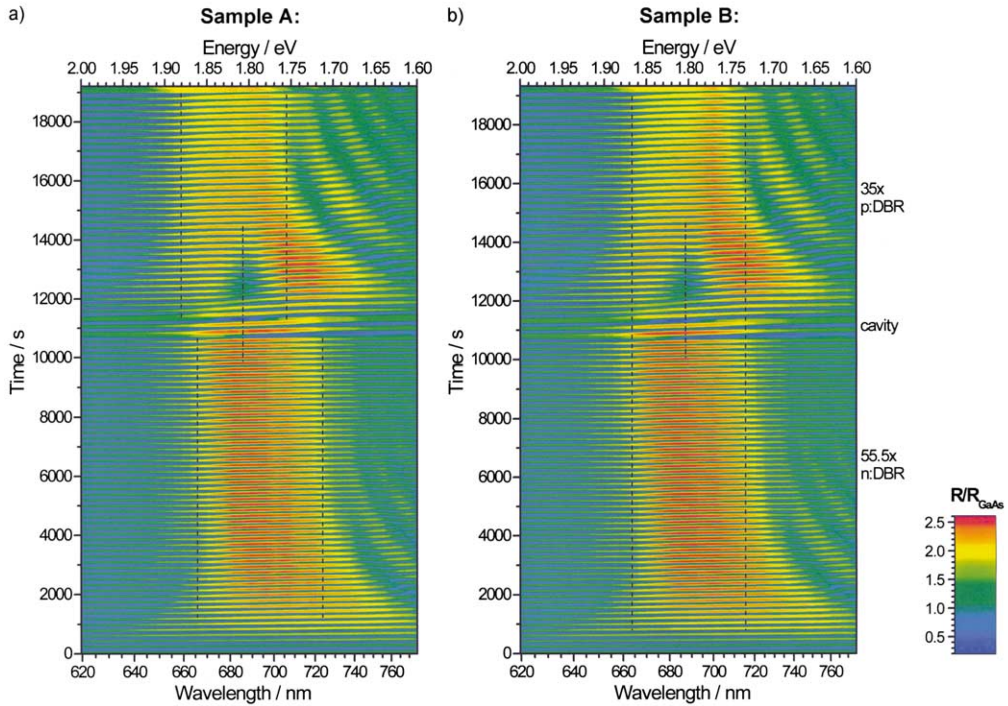

Fig. 8. Reflectance fingerprints of VCSEL samples A and B, showing the top and bottom DBR with the cavity in between. The spectroscopic positions of the stop bands and the cavity resonances are indicated by dashed lines.

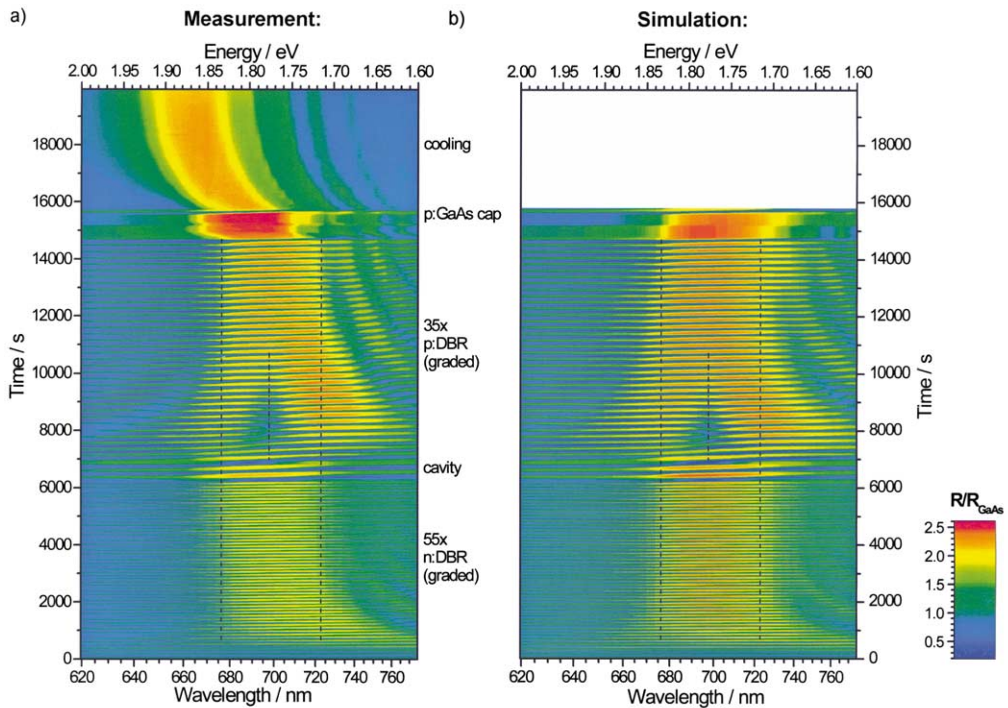

Fig. 9. Reflectance fingerprint of the complete VCSEL growth process: (a) as measured and (b) as calculated.

ization, can have tremendous effect to the electro-optic performance of the VCSEL device.

After carefully optimizing both the growth procedure and the processing of the 650 nm VCSEL structures a maximum output power of about 3 mW at room temperature was achieved.

Acknowledgements

The support for this work granted by the Deutsche Forschungsgemeinschaft (DFG) under contract TR357 and by the European Union (project ISCE-MOCVD) is gratefully acknowledged.

References

[1] J.L. Jewell, J.P. Harbison, A. Scherer, Y.H. Lee, L.T. Florez, IEEE J. Quant. Electron. 27 (1991) 1332.
[2] W.W. Chow, K.D. Choquette, M.H. Crawford, K.L. Lear, G.R. Hadley, IEEE J. Quant. Electron. 33 (1997) 1810.
[3] R.P. Schneider Jr., R.P. Bryan, J.A. Lott, E.D. Jones, G.R. Olbright, J. Crystal Growth 124 (1992) 763.
[4] D.E. Aspnes, Mater. Sci. Eng. B 30 (1995) 109.
[5] J.-T. Zettler, Prog. Cryst. Growth Charact. Mater. 35 (1997) 27.
[6] G.N. Maracas, J.L. Edwards, D.S. Gerber, R. Droopad, Appl. Surf. Sci. 63 (1993) 1.
[7] G. Böhm, M. Hauser, M. Sexl, G. Tränkle, G. Weimann, G. Abstreiter, SPIE 3286 (1998) 113.
[8] Y.M. Houng, M.R.T. Tan, B.W. Liang, S.Y. Wang, D.E. Mars, J. Vac. Sci. Technol. B 12 (1994) 1221.
[9] W.G. Breiland, H.Q. Hou, H.C. Chui, B.E. Hammons, J. Crystal Growth 174 (1997) 564.
[10] W.G. Breiland, K.P. Killeen, J. Appl. Phys. 78 (1995) 6726.
[11] M. Zorn, P. Kurpas, A.I. Shkrebtii, B. Junno, A. Bhattacharya, K. Knorr, M. Weyers, L. Samuelson, J.-T. Zettler, W. Richter, Phys. Rev. B 60 (1999) 8185.
[12] K. Haberland, A. Bhattacharya, M. Zorn, M. Weyers, J.-T. Zettler, W. Richter, J. Electron. Mater. 29 (2000) 468.
[13] M. Pristovsek, B. Han, J.-T. Zettler, W. Richter, J. Crystal Growth 221 (2000) 149.
[14] A. Bhattacharya, M. Zorn, A. Oster, M. Nasarek, H. Wenzel, J. Sebastian, M. Weyers, G. Tränkle, J. Crystal Growth 221 (2000) 663.
[15] K. Haberland, O. Hunderi, M. Pristovsek, J.-T. Zettler, W. Richter, Thin Solid Films 313–314 (1998) 620.
[16] K. Haberland, P. Kurpas, M. Pristovsek, J.-T. Zettler, M. Weyers, W. Richter, Appl. Phys. A 68 (1999) 309.
[17] J.-T. Zettler, K. Haberland, M. Zorn, M. Pristovsek, W. Richter, P. Kurpas, M. Weyers, J. Crystal Growth 195 (1998) 151.
[18] C.H. Kuo, S. Anand, H. Fathollahnejad, R. Ramamurti, R. Droopad, G.N. Maracas, J. Vac. Sci. Technol. B 13 (1995) 681.
[19] K. Haberland, T. Trepk, J.-T. Zettler, W. Richter, to be published.
[20] A. Oster, M. Zorn, K. Vogel, J. Fricke, J. Sebastian, W. John, M. Weyers, G. Tränkle, SPIE 4286 (2001) 148.
[21] K.L. Lear, R.P. Schneider Jr., Appl. Phys. Lett. 68 (1996) 605.
[22] A. Knigge, M. Zorn, H. Wenzel, M. Weyers, G. Tränkle, Electron. Lett. 37 (2001) 1222.
[23] K.D. Choquette, M.J. Hafich, M.H. Crawford, K.M. Geib, J.J. Hindi, IEEE Lasers and Electro-Optics Society 1999 12th Annual Meeting 2 (1999) 395, ISBN 0-7803-5634-9.
[24] J.A. Lott, L.V. Buydens, K.J. Malloy, K. Kobayashi, S. Ishikawa, Inst. Conf. Ser. 145 (1996) 973.